EDGE ARTICLE

Check for updates

All publication charges for this article have been paid for by the Royal Society of Chemistry

Effect of intramolecular energy transfer in a dual-functional molecular dyad on the performance of solution-processed TADF OLEDs†

Na Yeon Kwon,‡ Haeun Kwak,‡ Ha Yeon Kim,‡ Su Hong Park, Jin Young Park, Min Ji Kang, Chang Woo Koh, Sungnam Park, [ID] * Min Ju Cho*
and Dong Hoon Choi [ID] *

This paper introduces the design concept of a dual-functional molecular dyad tailored specifically for solution-processable organic light-emitting diodes (OLEDs). Cy-tmCPBN, characterized by an asymmetric molecular dyad structure, integrates a host unit (tmCP) and a multiple-resonance (MR) emitter (CzBN) *via* a non-conjugated cyclohexane linker. Cy-tmCPBN exhibited efficient intramolecular energy transfers (EnTs) from tmCP to the CzBN unit, as confirmed by time-resolved fluorescence experiments. The fluorescence lifetime of the tmCP unit was approximately three times shorter in a highly diluted solution of Cy-tmCPBN than in a mixed solution of Cy-tmCP and Cy-CzBN. In addition, Cy-tmCPBN exhibited excellent solubility and film-forming ability, making it suitable for solution processing. Notably, OLEDs utilizing Cy-tmCPBN achieved over twice the brightness and improved external quantum efficiency of 12.3% compared to OLEDs using Cy-CzBN with the same concentration of CzBN in the emitting layer. The improved OLED performance can be explained by the increased EnT efficiency from Cy-tmCP to Cy-tmCPBN and the intramolecular EnT within Cy-tmCPBN. In our dual-functional dyad, incorporating both host and emitter units in an asymmetric molecular dyad structure, we induced a positive synergy effect with the host moiety, enhancing OLED performance through intramolecular EnT.

Introduction

In the field of materials research related to organic photovoltaics (OPV) and organic light-emitting diodes (OLEDs), a profound understanding of photophysical and photochemical mechanisms, such as inter-/intramolecular energy transfer (EnT) and charge transfer (CT) through light irradiation, is crucial. Particularly, in the case of recently commercialized OLEDs, the light emission efficiency is induced based on the fundamental principle of intermolecular Förster resonance energy transfer (FRET) between the host and emitter molecules.[1–3] Furthermore, research on intermolecular CT, especially the study of exciplex hosts involving a combination of p-type and n-type hosts, has significantly contributed to the advancement of OLED technology.[4,5] These exciplex host systems allow the independent design of two organic semiconductor materials, leading to enhanced efficiency through balanced device mobility and a simplified device structure.[6–9] Additionally, recent studies have investigated thermally activated delayed fluorescence (TADF) emitters based on intramolecular space charge transfer (TSCT).[10–13]

However, the past photophysical strategy of intramolecular EnT has been predominantly focused on research involving the formation of intermolecular heterojunctions between donors and acceptors in organic photovoltaics.[14,15] In particular, the incorporation of both donors and acceptors within a single molecule to absorb solar energy in the active layer material has been studied, but the limitations in the performance of devices utilizing this approach have been recognized as challenging to overcome. Molecular dyads have been applied in various important applications, especially in the field of metal complexes and fluorescence molecules, serving as probes in biological research.[16–18] However, if a molecular dyad incorporates both organic semiconductor-based donor and acceptor elements and maintains an appropriate distance between the two semiconductor moieties to achieve efficient intramolecular EnT, it is anticipated to function as a crucial component in the emissive layer (EML) of OLEDs. Specifically, adopting the conjugative moiety used as a host in OLEDs as the donor and combining it with a desired emitter as the acceptor through an appropriate linker to form a molecular dyad, utilizing it as an

Department of Chemistry, Research Institute for Natural Sciences, Korea University, 145 Anam-ro, Seongbuk-gu, Seoul, 02841, Republic of Korea. E-mail: spark8@korea. ac.kr; chominju@korea.ac.kr; dhchoi8803@korea.ac.kr

† Electronic supplementary information (ESI) available. See DOI: https://doi.org/10.1039/d4sc02357a

‡ N. Y. Kwon, H. Kwak, and H. Y. Kim have equally contributed to this work.

emitter, may yield different effects on OLED performance compared to traditional physically blended host-emitter EML systems.

Recently, organic boron-based multiple resonance (MR) TADF emitters have attracted significant attention for their potential applications in wide gamut and high-resolution displays of OLEDs.[19–22] The MR effect, characterized by atomic-scale HOMO/LUMO separation, led to a minimal ΔE_{ST} and inhibited vibrational coupling between the S_0 and S_1 states. This resulted in a high photoluminescence quantum yield (PLQY) and narrowband emission with a reduced full-width-at-half-maximum (FWHM).[23–26] Therefore, given these advantages, it might be feasible to employ the previously mentioned molecular dyad as a medium-sized molecular emitter to develop narrowband OLEDs by integrating an MR emitter onto one or both branches of the molecular dyad.

MR-TADF emitters have been predominantly developed for vacuum-deposited emissive layers. Among them, BCzBN is one of the most widely used second-generation MR cores, and its planar solid structure leads to a narrow FWHM, making it widely applied in bright blue and green MR emitter structures.[27–31] However, the planar and rigid structure of MR-TADF emitters often facilitates the formation of weakly emitting aggregates or excimers.[32] Consequently, applying MR-TADF emitters in OLEDs reduces efficiency, shifts in electroluminescent (EL) wavelengths, and broadens the emission peak.[33] These undesirable issues become more pronounced when applied to solution-processed OLEDs. With growing interest in the benefits of solution processing for OLED fabrication, there is an urgent demand for comprehensive strategic research on MR-TADF emitters characterized by enhanced solubility and superior film-forming performance in organic solvents.

As previously stated, we opted for a structural approach employing a dual-functional molecular dyad with a nonconjugated linker to improve the solubility of the MR emitter and create an amorphous emitting layer. Based on earlier research employing this molecular design approach, both molecular dyad host materials and emitter molecules have demonstrated suitability as the EML in OLEDs fabricated via solution processes.[34–36]

Placing the same host moiety or MR emitter moiety on both branch locations enables the synthesis of a symmetric dyad. Through meticulous synthesis, it is possible to combine the host and emitter moieties on each branch to synthesize an asymmetric dyad.

By utilizing these three types of dyads, we can investigate the photoinduced intermolecular and intramolecular EnT phenomena through steady and time-resolved spectroscopic studies. By applying them to solution-processed OLEDs, we can compare the performance of an EML containing asymmetric molecular dyad emitters that exhibit intramolecular EnT with an asymmetric structure to that of a conventional EML based on a blend of molecular dyad hosts and emitters.

This study presents a dual-functional molecular dyad designed for efficient intramolecular EnT. More specifically, the recently developed Cy-tmCPBN utilizes a non-conjugated cyclohexane core to link the tmCP host and the CzBN emitter, preserving the distinct properties of both the host and emitter within the molecule. With a molecular weight exceeding 1000 g mol^{-1} and a three-dimensional structure, this dyad demonstrated enhanced solubility and excellent film-forming ability. Notably, Cy-tmCPBN efficiently exhibits intramolecular EnT from the tmCP moiety to the CzBN moiety. This feature is anticipated to have a significant impact on device performance when used in the EML of OLEDs. This advantage implies that both intramolecular and intermolecular EnT could occur in the subsequent device, suggesting that Cy-tmCP:Cy-tmCPBN-based OLEDs exhibiting unique narrowband emission could exhibit higher efficiencies than devices based on Cy-tmCP:Cy-CzBN, in which only intermolecular EnT occurs. As expected, Cy-tmCPBN-based OLEDs demonstrated superior device performance compared to OLEDs using the same concentration of Cy-CzBN.
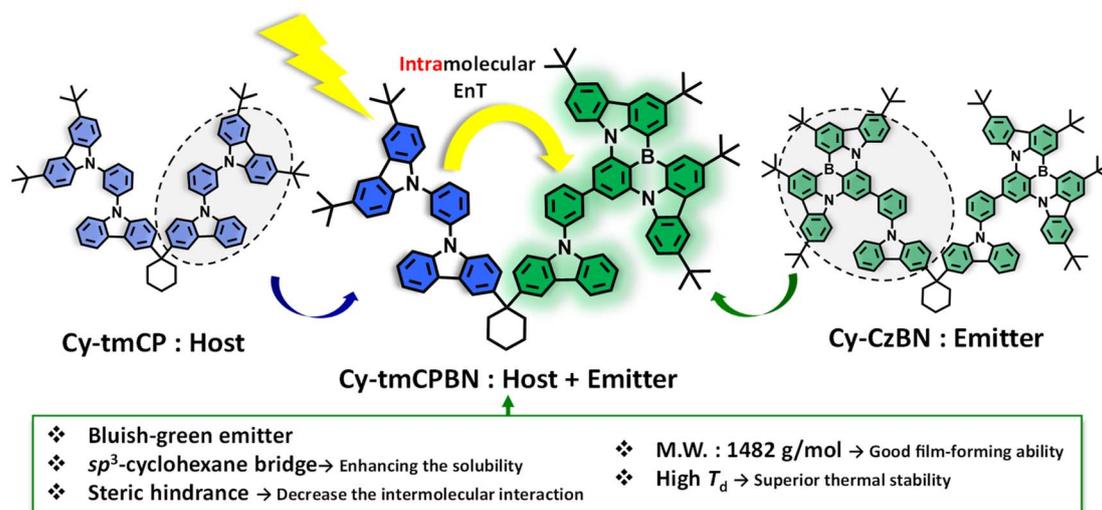

Fig. 1 Molecular design strategy for a solution-processable dual-functional molecular dyad with a cyclohexane linker.

This molecular dyad, proposed in this study, demonstrates intramolecular energy transfer and has the potential to exert positive synergy effects with the host within the EML of OLEDs, and enhancing energy transfer from the host moiety to the emitter (Fig. 1).

Results and discussion

Synthesis and molecular properties

To achieve the primary goal of this study, which was to synthesize a dual-functional dyad demonstrating intramolecular EnT, a host moiety used in the EML of OLEDs and a recently acclaimed narrowband emissive MR emitter were introduced into a single molecule. This was achieved by connecting the MR component (CzBN) and host component (tmCP) within a single molecule using cyclohexane as the sp³-linker. The *meta*-position was introduced to minimize the influence of carbazole derivatives linked to benzene at the *para*-position of the boron atom.

Consequently, the design of the molecular structure of Cy-tmCPBN aimed to maintain the independent features of the CzBN core without interference using a non-conjugated linker. In addition, we focused on preserving the unique properties associated with the MR emitter while facilitating intramolecular EnT within the molecular structure and ensuring narrowband emission. The key to achieving this goal is to maintain a close spatial proximity between tmCP and CzBN, allowing effective intramolecular EnT and ensuring the independent preservation of the emissive characteristics of the CzBN moiety within the molecule.

The synthetic routes to Cy-tmCP, Cy-CzBN, and Cy-tmCPBN are illustrated in Scheme S1.† The chemical structures of the three new molecular dyad materials were confirmed by ^{1}H, ^{13}C, and ^{11}B NMR spectroscopy (Fig. S1–S12†) and mass spectrometry (Fig. S13–S15†). These three compounds exhibited high solubilities in common organic solvents and demonstrated excellent film-forming properties. This is achieved by introducing six or eight *tert*-butyl substituents and a cyclohexane linker to obtain the desired molecular weight and solubility. In particular, Cy-tmCPBN demonstrated exceptional solubility even in hexane ($\geq$100 mg mL^{-1}).

These dyad materials displayed high decomposition temperatures (T_d, 5% weight loss) of 495 for Cy-tmCP, 523 for Cy-CzBN, and 529 °C for Cy-tmCPBN, respectively (Fig. S18a†). As shown in the DSC data in Fig. S20b,† both Cy-tmCP and Cy-tmCPBN exhibited glass transition temperatures (T_g) exceeding 240 °C, indicating that the cyclohexane bridge in the molecular dyad materials contributed to the enhancement of their thermal and morphological stabilities.

Theoretical calculations

Density functional theory (DFT) and time-dependent DFT (TD-DFT) methods were employed to obtain the optimized molecular structures, molecular orbitals (HOMO and LUMO), and natural transition orbitals (HONTO and LUNTO) of the molecular dyads used in this study. As presented in Fig. 2, the CzBN

units of Cy-tmCPBN and Cy-CzBN are responsible mainly for the HOMO and LUMO, and thus their HOMO and LUMO energies are very similar.

As confirmed by DFT calculations, the individual tmCP and CzBN units of the asymmetric molecular dyad tended to act independently because of their non-conjugated cyclohexane linkers. The energies of the four degenerate occupied molecular orbitals (from HOMO to HOMO−3) and the four unoccupied molecular orbitals (from LUMO to LUMO+3) of Cy-tmCP were almost identical, indicating that the four carbazole units in Cy-tmCP contributed equally to the frontier molecular orbitals (Fig. 2 and S16†). Similarly, Cy-CzBN exhibits equivalent energies for the frontier molecular orbitals (HOMO/HOMO−1 and LUMO/LUMO+1) because of the two identical CzBN units. Accordingly, the S$_1$ and S$_2$ energies of Cy-CzBN were identical; however, the two individual CzBN units contributed asymmetrically to the electronic transitions, as is clearly illustrated by the natural transition orbitals (HONTO and LUNTO; Fig. S18†). In particular, for Cy-CzBN, HONTO, and LUNTO, the S$_0$ → S$_1$ and S$_0$ → S$_2$ transitions were predominantly localized on the CzBN units.

In the case of Cy-tmCPBN, the electrochemical and photophysical properties of Cy-tmCPBN are primarily determined by the CzBN unit. Accordingly, the HOMO and LUMO energies, as well as the energies of the electronic states (S$_1$, T$_1$, and T$_2$), are nearly identical to those of Cy-CzBN except for the degenerate states (Fig. 2 and S19†). The tmCP unit in Cy-tmCPBN is commonly used as a host (Cy-tmCP) and facilitates energy transfer from the host to the emitting CzBN unit. In fact, the intramolecular EnT from the tmCP unit to the CzBN unit is highly efficient, as explained in detail below. In short, DFT calculations imply that the CzBN units in Cy-CzBN and Cy-tmCPBN are responsible for their optical and electrochemical properties and can play an important role as an emitting core in Cy-CzBN and Cy-tmCPBN.
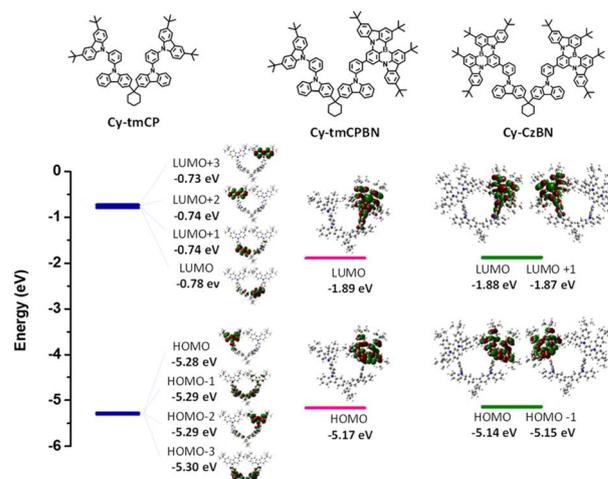

Fig. 2 Molecular structures and molecular orbitals of Cy-tmCP, Cy-tmCPBN, and Cy-CzBN obtained *via* DFT calculations (B3LYP/6-31G(d)).

Characterization of materials properties

The UV-visible absorption and photoluminescence (PL) spectra of the molecular dyads were measured in diluted toluene solutions at room temperature, as shown in Fig. 3. Their optical properties are listed in Table 1. Cy-CzBN and Cy-tmCPBN in toluene exhibited strong UV-visible absorption bands at 473 and 472 nm, respectively, owing to the short range CT transition of the CzBN unit. For Cy-tmCP, a PL peak was observed at 355 nm, which resulted from the emission of the mCP unit. In contrast, Cy-CzBN exhibited bluish-green emission at 494 nm with a bandwidth of 22 nm.[37] Cy-tmCPBN showed a PL peak at 491 nm with a bandwidth of 22 nm, resulting from the CzBN unit of Cy-tmCPBN.

We investigated the photophysical characteristics of BCzBN, Cy-CzBN, and Cy-tmCPBN neat films and doped films by measuring their PL spectra in more detail. In Fig. 3b, the neat film of BCzBN exhibits a broad shoulder peak at ~570 nm, which was not observed in the neat films of Cy-CzBN and Cy-tmCPBN. This is interpreted as the mitigation of aggregation between emitter molecules facilitated by the introduction of a three-dimensional sp[3] linker.
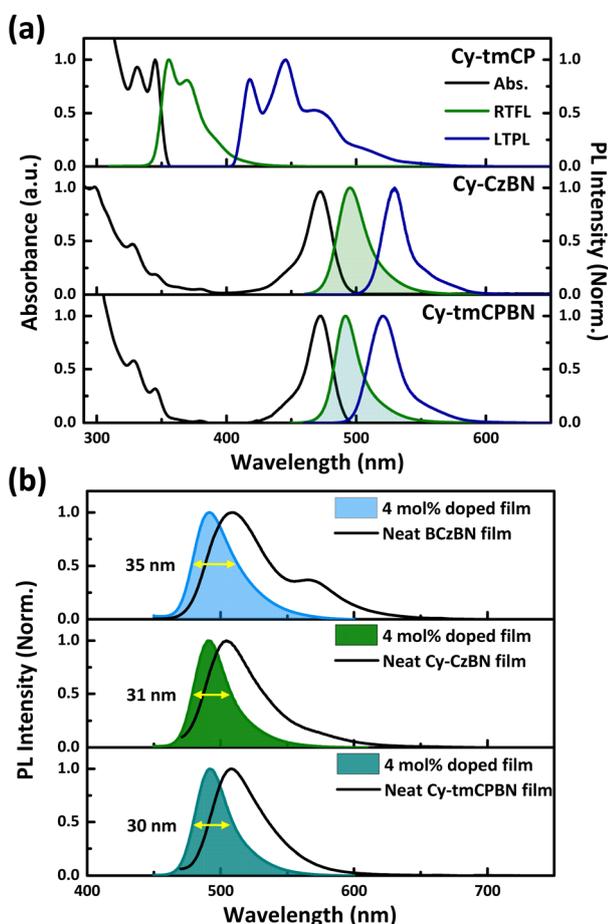

Fig. 3 (a) UV-visible absorption (Abs), fluorescence (FL), phosphorescence (Phos) spectra in toluene (1×10^{-5} M) at 300 K and 77 K. (b) FL spectra of neat Cy-CzBN and Cy-tmCPBN films and 4 mol% doped Cy-tmCP films.

To investigate intramolecular EnT in Cy-tmCPBN, we prepared two diluted toluene solutions (1×10^{-7} M) containing only Cy-tmCPBN and a mixture of Cy-tmCP and Cy-CzBN in a 1 : 1 molar ratio. As shown in Fig. 4a, the PL spectra of a mixture of Cy-tmCP and Cy-CzBN in toluene revealed distinct individual PL peaks resulting from tmCP and CzBN, respectively. In contrast, the PL spectrum of Cy-tmCPBN in toluene displayed a negligibly small PL peak at 355 nm and a large PL peak at 491 nm, indicating efficient intramolecular EnT from the tmCP unit to the CzBN unit in Cy-tmCPBN.

To investigate the intramolecular EnT in more detail, we measured the time-resolved fluorescence (TRF) signals of Cy-tmCPBN and a mixture of Cy-tmCP and Cy-CzBN in toluene (1×10^{-7} M), as shown in Fig. 4b. Fig. 4b shows the TRF signals of the tmCP units in the two solutions, measured at 355 nm. The TRF signal of Cy-tmCPBN decayed much faster than that of the mixture of Cy-tmCP and Cy-CzBN, which resulted from intramolecular EnT from the tmCP unit to the CzBN unit in Cy-tmCPBN. The TRF signals were fitted using a bi-exponential function and the average lifetimes (τ_{avg}) were extracted. Using a simple kinetic model in Fig. 4c, the intramolecular EnT rate constants (k_{ET}) were determined. In Cy-tmCPBN, the intramolecular EnT from the tmCP unit to the CzBN unit was twice as fast as the fluorescence relaxation of the tmCP unit ($k_{ET} = 3.9 \times 10^8$ s^{-1} $vs.$ $k_1 = 1.9 \times 10^8$ s^{-1}). The TRF signals of the CzBN units in the two dilute solutions were almost identical (Fig. S24†).

To study the impact of emitter concentrations on the intramolecular EnT, over the range from 2 mol% to 12 mol% of doped Cy-CzBN and Cy-tmCPBN films were prepared in Cy-tmCP. Fig. S22a and d† show the emission spectra of the doped Cy-CzBN and Cy-tmCPBN films. The intensities of Cy-CzBN and Cy-tmCPBN decreased as the concentration increased up to 12%.

However, a difference was revealed in the normalized steady-state emission spectra of both films, which was a difference in intensity at approximately 350–400 nm. Unlike Cy-CzBN, Cy-tmCPBN exhibited a consistent intensity in the 350–400 nm range, regardless of the doping concentration, which was attributed to intramolecular EnT from tmCP to the CzBN unit.

In addition, the TRF signals of Cy-CzBN- and Cy-tmCPBN-doped Cy-tmCP films were measured at the PL peak (488 nm) of the CzBN units (Fig. S25†). The TRF signal of Cy-tmCPBN-doped films decayed slightly faster than that of Cy-CzBN-doped films, indicating that the PL of the CzBN units was more efficient in Cy-tmCPBN-doped Cy-tmCP films than Cy-CzBN-doped Cy-tmCP films. In the films, two nearby CzBN units in Cy-CzBN can undergo intramolecular energy exchange, which may slow the overall energy relaxation.

In the Cy-tmCP:Cy-CzBN system, the blended film of the two materials represented an interface between two molecules of medium-size, allowing for phase separation. Nevertheless, intermolecular EnT from tmCP to CzBN was quite efficient in the blend film prepared at room temperature. However, for the Cy-tmCP:Cy-tmCPBN blend film, the interface between the two medium-sized molecules in the film was expected to be exceptionally well formed because of the common inclusion of the

Table 1 Photophysical and electrochemical properties for Cy-tmCP, Cy-CzBN, and Cy-tmCPBN

Compound	$\lambda_{abs}{}^a$ (nm)	$\lambda_{PL}{}^a$ (nm)	FWHM^a (nm)	$E_S/E_T/\Delta E_{ST}{}^b$ (eV)	$E_{HOMO}/E_{LUMO}{}^c$ (eV)	$\Phi_{PL}{}^d$ (%)
Cy-tmCP	298, 345	355	30	3.61/3.06/0.55	−5.69/−2.19	11.7
Cy-CzBN	299, 473	494	22	2.61/2.43/0.18	−5.54/−3.08	57.3
Cy-tmCPBN	297, 472	491	22	2.62/2.50/0.12	−5.60/−3.13	65.4

^{a} Measured in toluene (1×10^{-5} M). ^{b} E_S and E_T energies were obtained from the onset of the fluorescence and phosphorescence spectra in toluene at 298 K and 77 K, respectively. ^{c} E_{HOMO} (eV) $= -e(4.8 \text{ eV} + E_{ox} - E_{ferrocene})$ and E_{LUMO} (eV) $= E_{HOMO}$ (eV) $+ E_g$ (eV). ^{d} Overall absolute PLQY obtained in 4 mol% doped thin film with an Cy-tmCP host using an integrating sphere.

tmCP moiety in both molecules, indicating outstanding miscibility. Therefore, based on the results of the steady-state emission and transient PL spectra, it was confirmed that both inter- and intramolecular EnTs were possible within the film in this case.

When the solvent was changed from nonpolar hexane to polar chloroform (Fig. S27†), Cy-tmCPBN exhibited a solvent-dependent shift in a manner similar to Cy-CzBN, with only a slight 10 nm bathochromic shift in emission (Table S1†). This suggests that, in the excited state, the tmCP unit does not significantly alter the MR emission characteristics of Cy-tmCPBN and Cy-CzBN.

Furthermore, cyclic voltammetry (CV) measurements were conducted to determine the HOMO energy levels of molecular dyads (Fig. S28 and Table S2†). In the solution state, the oxidation onset potential of Cy-tmCPBN was identical to that of Cy-CzBN (+1.00 V). However, in the film state, the oxidation potential of Cy-tmCPBN was measured at +1.13 V, which falls between the values for Cy-tmCP (+1.22 V) and Cy-CzBN (+1.07 V).

The HOMO energy level of Cy-tmCPBN was determined to be −5.60 eV, with the LUMO level calculated at −3.13 eV. The LUMO energy level was estimated from the optical bandgap and HOMO energy. These findings aligned with the DFT calculations illustrated in Fig. 2, suggesting a significant impact of the CzBN segment on the energy characteristics of Cy-tmCPBN, as corroborated by experimental observations.

Surface morphology analysis

The surface morphology of the solution-processed EML was investigated using atomic force microscopy (AFM), as depicted in Fig. S29.† The overall root mean square (RMS) of the thin film indicated a uniformly smooth surface of less than 1.0 nm. Fig. S29a and b† illustrated the film surfaces of the individual materials; the surface of a neat thin film of Cy-tmCPBN
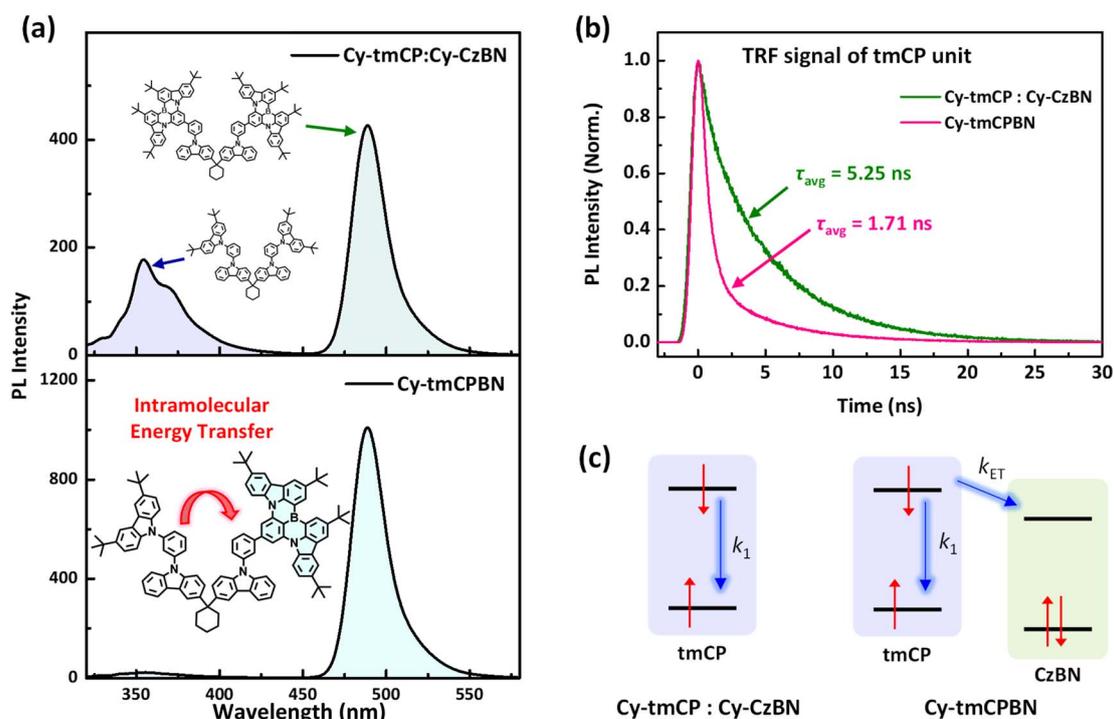

Fig. 4 (a) Steady-state fluorescence spectra and (b) time-resolved fluorescence (TRF) signals were measured at 355 nm (λ_{ex} = 340 nm) of blend (Cy-tmCP : Cy-CzBN = 1 : 1 mol ratio) and Cy-tmCPBN diluted toluene solution (1×10^{-7} M) at 300 K. (c) Kinetic model illustrating the intramolecular energy transfer from tmCP unit to CzBN unit in Cy-tmCPBN. ($k_1 = 1.9 \times 10^8$ s^{-1} and $k_{ET} = 3.9 \times 10^8$ s^{-1}).

exhibited a morphology similar to Cy-tmCP (Fig. S29c†), with a roughness of 0.263 nm. The blend films of Cy-tmCP:Cy-tmCPBN displayed a very fine surface morphology. In contrast, the film containing Cy-tmCP:Cy-CzBN exhibited a relatively rough surface with an RMS roughness of 0.313 nm and large domain size.

Consequently, the thin film containing Cy-tmCPBN exhibited a fine surface morphology. The finer morphology suggested that effective CT was anticipated in the EML, which was attributed to the shared presence of tmCP and the facilitated compatibility between the Cy-tmCP and Cy-tmCPBN molecules.

Performance of the solution-processed TADF-OLEDs

After investigating the optical and photophysical properties of the molecular dyads, we fabricated OLEDs using a solution-processing technique to observe their electroluminescence characteristics. The OLED structure was ITO/PEDOT:PSS (30 nm)/PX2Cz (20 nm)/Cy-tmCP:x mol% MR emitter (20 nm) (x = 2–12 mol%)/BmPyPB (50 nm)/LiF (1 nm)/Al (100 nm). PEDOT:PSS, PX2Cz, BmPyPB, and LiF were used as the hole injection, hole transport, electron transport, and electron injection layers, respectively. The photocrosslinked PX2Cz ensured desirable energy levels for EML fabrication and durability in the organic solvent of the HTL.[38] The materials employed in the OLEDs are illustrated in Fig. 5b, while Fig. 5a displays the corresponding device structure and energy diagram. To optimize and analyze the performance of the OLED devices, we fabricated devices with various doping concentrations (2–12 mol%) of Cy-CzBN and Cy-tmCPBN. The device characteristics are presented in Fig. 5 and S31,† and the corresponding performance parameters are listed in Table 2.

As the emitter (CzCN moiety) concentration increased from 2 to 12 mol%, no significant change was observed in the maximum external quantum efficiency (EQE$_{max}$) during measurement in both Cy-tmCP:Cy-CzBN and Cy-tmCP:Cy-tmCPBN devices, indicating that the molecular dyad structure of the emitters can suppress aggregation-induced quenching with increasing emitter concentration. Additionally, devices based on Cy-tmCPBN exhibited higher EQE$_{max}$ and a smaller efficiency roll-off compared to those based on Cy-CzBN. The EQE$_{max}$ of the Cy-tmCPBN-based device reached 12.33%, with efficiency roll-offs of 23.52% and 43.83% at luminances of 100 cd m^{-2} and 200 cd m^{-2}, respectively. In contrast, the Cy-CzBN-based device showed an EQE$_{max}$ of 10.90%, with efficiency roll-offs of 50.19% and 67.44% at the same luminances. When evaluating the molecular orientation of the EML, both systems displayed similar values (Fig. S32†). This suggests that the emitter orientation effects can be assumed to be similar in explaining the observed performance differences between the two devices. As a result, the enhanced performance and reduced efficiency roll-off of Cy-tmCPBN-based devices are attributed to shorter τ_d, more efficient EnT, and superior PLQY of the doped EML.

As shown in Fig. S22,† increasing the concentration of the emitter in the two different OLEDs resulted in an increase in the FWHM of the EML spectrum, and the emission wavelength shifted towards longer wavelengths. Upon closer examination, it was evident that the variation in the EML spectra of the blend films containing Cy-tmCP and Cy-CzBN was more pronounced with respect to the emitter concentration. This is particularly notable when high concentrations of Cy-CzBN, which contains two emitter moieties, are doped into the Cy-tmCP host. In such cases, the enhanced interaction between the neighboring CzBN
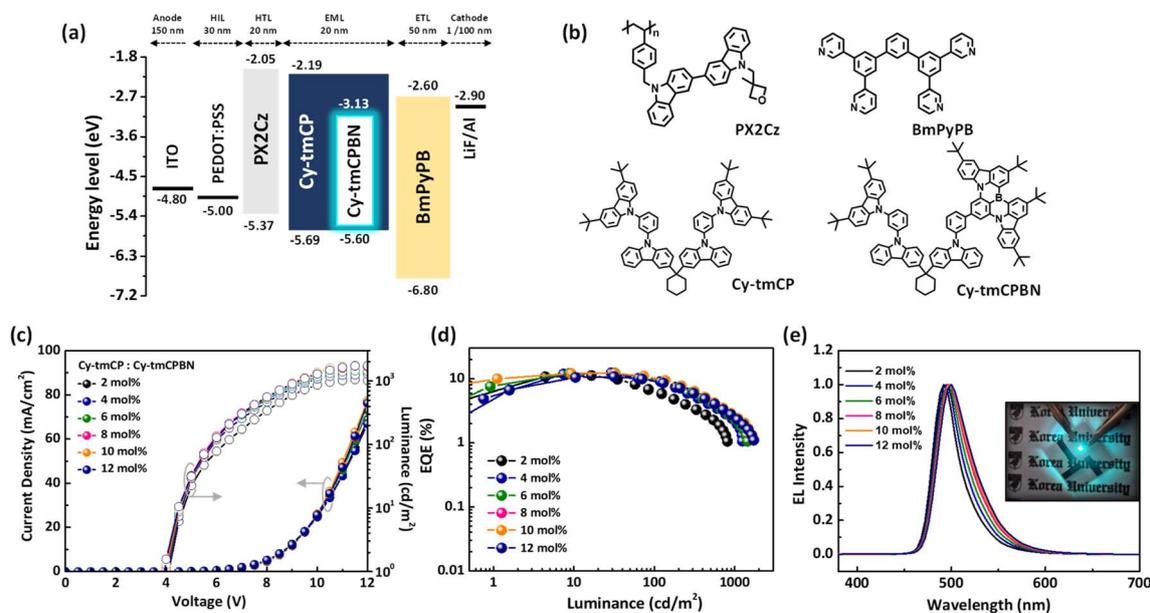

Fig. 5 (a) Device configurations and energy diagram of the solution-processed TADF-OLEDs. (b) The chemical structure of the materials used in the devices. (c) Current density–voltage–luminance (J–V–L) curves and (d) external quantum efficiency (EQE) curves of the devices. (e) EL spectra of the Cy-tmCP films doped with x mol% Cy-tmCPBN (x = 2–12 mol%)—insets photograph: 4 mol% Cy-tmCPBN-based device.

Table 2 EL performance of the solution-processed TADF-OLEDs based on Cy-tmCP:x mol% Cy-tmCPBN ($x = 2$–12 mol%)

Doping conc. (mol%)	$V_{on}{}^a$ (V)	$\eta_{c,max}{}^b$ (cd A^{-1})	$\eta_{p,max}{}^c$ (Lm W^{-1})	L^d (cd m^{-2})	$\eta_{ext,max}{}^e$ (%)	$\lambda_{EL}{}^f$ (nm)	FWHM (nm)	CIE^g (x, y)
2	4.07	23.94	16.08	809	11.21	492	32	(0.10, 0.45)
4	4.01	28.30	19.22	1291	12.33	496	36	(0.11, 0.50)
6	4.00	30.10	20.91	1444	12.26	496	38	(0.12, 0.53)
8	3.94	31.37	21.90	1711	12.14	496	40	(0.13, 0.55)
10	3.88	31.29	21.03	1745	11.86	500	41	(0.14, 0.56)
12	3.81	29.06	19.77	1732	10.74	500	43	(0.14, 0.57)

^{a} Turn-on voltage of 1 cd m^{-2}. ^{b} Maximum CE. ^{c} Maximum PE. ^{d} Maximum luminance. ^{e} Maximum EQE. ^{f} EL peak wavelength. ^{g} CIE color coordinates at 1000 cd m^{-2}.

emitters and host materials can influence electronic transitions, potentially having a more significant impact on the wavelength of the emitted light.

Thus, the introduction of various MR-TADF emitter units and a host moiety at the two branch positions within the asymmetric molecular dyad structure independently demonstrated dual functionality. Based on the results regarding the device performance mentioned above, this suggests a significant advantage in realizing high-efficiency, solution-processable OLEDs.

Conclusion

In this study, we successfully synthesized Cy-tmCPBN, a solution-processable MR-TADF emitter that simultaneously incorporates both the tmCP host moiety and the CzBN-emitting moiety. We achieved our research goal of enabling efficient intramolecular energy transfer while preserving the MR-TADF properties that exhibit narrowband emission. The advantages of molecular dyad structures such as Cy-tmCP, Cy-CzBN, and Cy-tmCPBN have been confirmed through their high solubility, excellent thermal stability, and morphological stability within the film. Particularly, for Cy-tmCPBN, the absorption and emission characteristics were primarily attributed to the CzBN moiety, and efficient intramolecular energy transfer from tmCP to CzBN was observed. Time-resolved fluorescence experiments showed that the lifetime of tmCP in Cy-tmCPBN was approximately three-fold shorter than that in Cy-tmCP because of efficient intramolecular energy transfer. In the solution-processed OLEDs, even when the emitter concentration in the Cy-tmCPBN-based OLEDs was changed from 2 mol% to 12 mol%, similarly high EQE$_{max}$ values were observed. These results suggest that the molecular design strategy of introducing various MR-TADF emitter units into the dual-functional molecular dyad structure is promising for the future implementation of high-efficiency solution-processable OLEDs.

Data availability

The data (instrumentation, synthetic procedures, structural characterization data, theoretical calculations, spectroscopic data, and device performance data) that support this article is available in the article itself and its ESI.†

Author contributions

N. Y. K., H. K. and H. Y. K. contributed equally to this work. N. Y. K. and H. K. – conceptualization, investigation, OLED devies, writing – original draft; H. Y. K., C. W. K. and S. P. – theoretical calculation, investigation (time-resolved PL study); S. H. P. – formal analysis, OLED devices; J. Y. P. and M. J. K. – investigation (thermal properties); S. P., M. J. C., and D. H. C. – project administration, supervision, writing – review & editing.

Conflicts of interest

There are no conflicts to declare.

Acknowledgements

References

1 P. Heimel, A. Mondal, F. May, W. Kowalsky, C. Lennartz, D. Andrienko and R. Lovrincic, *Nat. Commun.*, 2018, **9**, 4990.

2 D. Zhang, L. Duan, D. Zhang and Y. Qiu, *J. Mater. Chem. C*, 2014, **2**, 8983–8989.

3 T. Furukawa, H. Nakanotani, M. Inoue and C. Adachi, *Sci. Rep.*, 2015, **5**, 8429.

4 Q. Wang, Q.-S. Tian, Y.-L. Zhang, X. Tang and L.-S. Liao, *J. Mater. Chem. C*, 2019, **7**, 11329–11360.

5 Y. S. Park, S. Lee, K. H. Kim, S. Y. Kim, J. H. Lee and J. J. Kim, *Adv. Funct. Mater.*, 2013, **23**, 4914–4920.

6 C. J. Shih, C. C. Lee, T. H. Yeh, S. Biring, K. K. Kesavan, N. R. A. Amin, M. H. Chen, W. C. Tang, S. W. Liu and K. T. Wong, *ACS Appl. Mater. Interfaces*, 2018, **10**, 24090–24098.

7 J. H. Lee, S. H. Cheng, S. J. Yoo, H. Shin, J. H. Chang, C. I. Wu, K. T. Wong and J. J. Kim, *Adv. Funct. Mater.*, 2014, **25**, 361–366.

8 D. Kolosov, V. Adamovich, P. Djurovich, M. E. Thompson and C. Adachi, *J. Am. Chem. Soc.*, 2002, **124**, 9945–9954.

9 T. Xu, Y. X. Zhang, B. Wang, C. C. Huang, I. Murtaza, H. Meng and L. S. Liao, *ACS Appl. Mater. Interfaces*, 2017, **9**, 2701–2710.

10 X. Lv, Y. Wang, N. Li, X. Cao, G. Xie, H. Huang, C. Zhong, L. Wang and C. Yang, *Chem. Eng. J.*, 2020, **402**, 126173.

11 Y. K. Wang, C. C. Huang, H. Ye, C. Zhong, A. Khan, S. Y. Yang, M. K. Fung, Z. Q. Jiang, C. Adachi and L. S. Liao, *Adv. Opt. Mater.*, 2019, **8**, 1901150.

12 H. Tsujimoto, D. G. Ha, G. Markopoulos, H. S. Chae, M. A. Baldo and T. M. Swager, *J. Am. Chem. Soc.*, 2017, **139**, 4894–4900.

13 X. Wang, S. Wang, J. Lv, S. Shao, L. Wang, X. Jing and F. Wang, *Chem. Sci.*, 2019, **10**, 2915–2923.

14 A. Ajayaghosh, S. J. George and V. K. Praveen, *Angew. Chem.*, 2003, **115**, 346–349.

15 A. a. F. Eftaiha, J.-P. Sun, I. G. Hill and G. C. Welch, *J. Mater. Chem. A*, 2014, **2**, 1201–1213.

16 Z. Wang, T. D. Cong, W. Zhong, J. W. Lau, G. Kwek, M. B. Chan-Park and B. Xing, *Angew. Chem., Int. Ed.*, 2021, **60**, 16900–16905.

17 S. Leroy-Lhez, J. Baffreau, L. Perrin, E. Levillain, M. Allain, M.-J. Blesa and P. Hudhomme, *J. Org. Chem.*, 2005, **70**, 6313–6320.

18 X. Jia, Q. Chen, Y. Yang, Y. Tang, R. Wang, Y. Xu, W. Zhu and X. Qian, *J. Am. Chem. Soc.*, 2016, **138**, 10778–10781.

19 X. Liang, Z. P. Yan, H. B. Han, Z. G. Wu, Y. X. Zheng, H. Meng, J. L. Zuo and W. Huang, *Angew. Chem.*, 2018, **130**, 11486–11490.

20 H. J. Cheon, Y.-S. Shin, N.-H. Park, J.-H. Lee and Y.-H. Kim, *Small*, 2022, **18**, 2107574.

21 J. Wang, N. Li, C. Zhong, J. Miao, Z. Huang, M. Yu, Y. X. Hu, S. Luo, Y. Zou, K. Li and C. Yang, *Adv. Mater.*, 2023, **35**, 2208378.

22 D. Sun, S. M. Suresh, D. Hall, M. Zhang, C. Si, D. B. Cordes, A. M. Slawin, Y. Olivier, X. Zhang and E. Zysman-Colman, *Mater. Chem. Front.*, 2020, **4**, 2018–2022.

23 N. Ikeda, S. Oda, R. Matsumoto, M. Yoshioka, D. Fukushima, K. Yoshiura, N. Yasuda and T. Hatakeyama, *Adv. Mater.*, 2020, **32**, e2004072.

24 T. Hua, J. Miao, H. Xia, Z. Huang, X. Cao, N. Li and C. Yang, *Adv. Funct. Mater.*, 2022, **32**, 1372.

25 J.-M. Teng, Y.-F. Wang and C.-F. Chen, *J. Mater. Chem. C*, 2020, **8**, 11340–11353.

26 M. Yang, S. Shikita, H. Min, I. S. Park, H. Shibata, N. Amanokura and T. Yasuda, *Angew. Chem., Int. Ed.*, 2021, **60**, 23142–23147.

27 Y. Zhang, D. Zhang, J. Wei, Z. Liu, Y. Lu and L. Duan, *Angew. Chem., Int. Ed.*, 2019, **58**, 16912–16917.

28 S. Xu, Q. Yang, Y. Zhang, H. Li, Q. Xue, G. Xie, M. Gu, J. Jin, L. Huang and R. Chen, *Chin. J. Chem.*, 2021, **32**, 1372–1376.

29 M. Yang, I. S. Park and T. Yasuda, *J. Am. Chem. Soc.*, 2020, **142**, 19468–19472.

30 Y. Xu, Z. Cheng, Z. Li, B. Liang, J. Wang, J. Wei, Z. Zhang and Y. Wang, *Adv. Opt. Mater.*, 2020, **8**, 1902142.

31 X. F. Luo, H. X. Ni, X. Liang, D. Yang, D. Ma, Y. X. Zheng and J. L. Zuo, *Adv. Opt. Mater.*, 2023, **11**, 2203002.

32 D. Hall, K. Stavrou, E. Duda, A. Danos, S. Bagnich, S. Warriner, A. M. Z. Slawin, D. Beljonne, A. Kohler, A. Monkman, Y. Olivier and E. Zysman-Colman, *Mater. Horiz.*, 2022, **9**, 1068–1080.

33 Y. Zhang, J. Wei, D. Zhang, C. Yin, G. Li, Z. Liu, X. Jia, J. Qiao and L. Duan, *Angew. Chem., Int. Ed.*, 2022, **61**, e202113206.

34 I. S. Park, H. Seo, H. Tachibana, J. U. Kim, J. Zhang, S. M. Son and T. Yasuda, *ACS Appl. Mater. Interfaces*, 2017, **9**, 2693–2700.

35 D. W. Lee, J. Hwang, H. J. Kim, H. Lee, J. M. Ha, H. Y. Woo, S. Park, M. J. Cho and D. H. Choi, *ACS Appl. Mater. Interfaces*, 2021, **13**, 49076–49084.

36 N. Y. Kwon, S. H. Park, C. W. Koh, J. Y. Park, M. J. Kang, H. I. Baek, J. Youn, S. Park, C. W. Han, M. J. Cho and D. H. Choi, *ACS Appl. Mater. Interfaces*, 2023, **15**, 28277–28287.

37 M.-S. Lin, S.-J. Yang, H.-W. Chang, Y.-H. Huang, Y.-T. Tsai, C.-C. Wu, S.-H. Chou, E. Mondal and K.-T. Wong, *J. Mater. Chem.*, 2012, **22**, 16114.

38 J. H. Lee, C. H. Jeong, M. Godumala, C. Y. Kim, H. J. Kim, J. H. Hwang, Y. W. Kim, D. H. Choi, M. J. Cho and D. H. Choi, *J. Mater. Chem. C*, 2020, **8**, 4572–4579.